Late twentieth century Northern Hemisphere sea-ice record from U.S. National Ice Center ice charts

Kim Partington
Vexcel UK, Newbury, Berkshire, UK

Tom Flynn
Vexcel Corporation, Boulder, Colorado, USA

Doug Lamb, Cheryl Bertoia,[1] and Kyle Dedrick
National/Naval Ice Center, Washington, D. C., USA

Received 2 September 2002; revised 20 May 2003; accepted 11 August 2003; published 6 November 2003.

[1] Arctic sea ice plays a key role in the climate system, by acting as the interface between a warm ocean and a cold atmosphere. Establishing the true pattern of recent behavior of the sea ice in this region is critical to simulating the role of sea ice in future climate. Recently released operational ice charts from the U.S. National Ice Center provide insight into the late twentieth century behavior of Northern Hemisphere sea ice, providing more reliable ice concentrations during summer and freeze-up than those available from the passive microwave record. The major winter and summer modes of ice concentration variability observed from empirical orthogonal function analysis covering the period 1972–1994 are shown to indicate, respectively, the 1-year lagged response of the sea ice to the North Atlantic Oscillation and the winter preconditioning of summer sea ice coverage in the eastern Arctic by the North Atlantic Oscillation. Feedback to the atmosphere is suggested in each case by zero-lag cyclone frequency relationships to these two sea ice modes of variability. *INDEX TERMS:* 1620 Global Change: Climate dynamics (3309); 4215 Oceanography: General: Climate and interannual variability (3309); 1640 Global Change: Remote sensing; 3349 Meteorology and Atmospheric Dynamics: Polar meteorology;
KEYWORDS: sea ice, climate, ice charts, empirical orthogonal functions

Citation: Partington, K., T. Flynn, D. Lamb, C. Bertoia, and K. Dedrick, Late twentieth century Northern Hemisphere sea-ice record from U.S. National Ice Center ice charts, *J. Geophys. Res.*, *108*(C11), 3343, doi:10.1029/2002JC001623, 2003.

1. Introduction

[2] During the last decade, it has become steadily more apparent that there are significant and widespread changes occurring across the Arctic, including a 5.2% reduction in sea ice extent across the Northern Hemisphere between 1978 and 1996 (2.9% per decade [*Cavalieri et al.*, 1997]) and a reduction of 14% in the extent of multiyear ice in the last 2 decades, equivalent to a reduction in the mean age of sea ice [*Johannessen et al.*, 1995]. These observations are consistent with an observed increase in the winter ice flux through the Fram Strait [*Kwok and Rothrock*, 1999] and a decline in the mean thickness of sea ice from the 1970s to the 1990s [*Rothrock et al.*, 1999].

[3] The significance of these changes in terms of anthropogenic and other forcings can only be addressed effectively through the acquisition of data sets that have hemispheric coverage. Passive microwave sensors from the U.S. Defense Meteorological Satellite Program have long provided a key source of information on Arctic-wide sea ice conditions, but suffer from some known deficiencies, notably a tendency to underestimate ice concentrations in summer. With the recent release of digital and quality controlled ice charts extending back to 1972 from the U.S. National Ice Center (NIC), there is now an alternative record of late twentieth century Northern Hemisphere sea ice conditions to compare with the valuable, but imperfect, passive microwave sea ice record.

2. The U.S. National Ice Center Ice Charts

2.1. Background

[4] The NIC ice chart data are derived from operational ice charts used to guide both military and commercial operations in ice-infested waters (Figure 1). The origins of the ice charting activity, and the U.S. Navy-National Oceanographic and Atmospheric Administration-U.S. Coast Guard cooperation, lie in post-WW2 accidents and near-accidents involving sea ice [*Benner and Ramsay*, 2000]. These ice charts, originally in paper form and now in digital form, cover almost all of the ice-infested ocean waters of the Northern and Southern Hemispheres. In the Northern Hemi-

[1]Now at Cospas-Sarsat Secretariat, London, UK.

0148-0227/03/2002JC001623$09.00

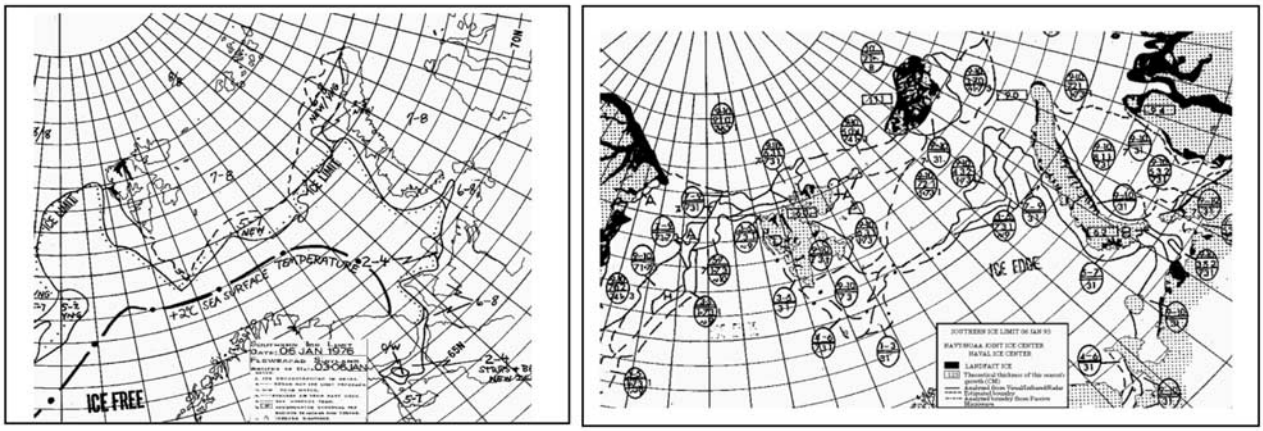

Figure 1. Examples of U.S. National Ice Center ice charts from (left) 1976 and (right) 1993, representing examples of early and recent ice charts associated with the data set used in this study. The ''eggs'' represent standard WMO conventions for representing sea ice information. The top number in the egg is total ice concentration.

sphere, these ice charts have been produced routinely on a weekly basis and formatted according to World Meteorological Organisation standards (World Meteorological Organisation Sea-Ice Nomenclature, WMO 259.TP.145).

[5] In the early 1990s, there was a high level initiative to enhance United States-Russia cooperation in science. A result of this was the Environmental Working Group Joint U.S.-Russian Arctic Sea Ice Atlas, compiled by the NIC and the Arctic and Antarctic Research Institute (AARI) in St. Petersburg, Russia. A major component of this atlas is the digital sea ice charts provided by NIC and released in October 2000, and it is this component of the Arctic Sea Ice Atlas that represents the focus for this paper. We analyze total ice concentrations from the data set. Hardcopy ice charts exist from before 1972, but these are not in a form which is convenient for quantitative analysis, while other ice information, in particular related to partial ice concentrations, may have some value but are temporally and spatially inconsistent in quality and therefore inappropriate for analysis of sea ice variability over the period of interest.

2.2. Production of the Ice Charts

[6] Details about the generation of ice charts at the U.S. National Ice Center are provided in *Dedrick et al.* [2001], and we will provide only a brief outline here. The ice charts have grown from being relatively coarse products in 1972 to detailed and comprehensive charts by the mid 1990s, reflecting the increasing range of data sources available to the analysts (compare the charts in Figure 1). During the 1970s, the data sources included the TIROS-N series of satellites (initially VHRR, and later AVHRR) along with ship-borne and aerial reconnaissance data. Nimbus 5 19.35-GHz passive microwave data were available from 1972 to 1980, and output from the ESMR single-channel ice algorithm was used in hardcopy form (Tom Wilheit, personal communication, 2002). By the beginning of the 1980s, visual, infrared, and passive microwave sensors on board the Defense Meteorological Satellite Program (DMSP) satellites were available. It is not clear at what point the ESMR/NASA single channel algorithm was replaced by the U.S. Navy CAL/VAL algorithm, but this could have been as late as 1989 when the definition of the algorithm was published [see *Hollinger et al.*, 1991]. The ''CAL/VAL'' algorithm is a U.S. Navy algorithm designed to provide a realistic ice edge position by emphasizing use of the 37-GHz channel [*Benner and Bertoia*, 1992]. It does this at the cost of precision within the pack where ice concentrations become saturated. The value of passive microwave data is that it is able to ''see'' through clouds, albeit at a coarse resolution of the order of 25 km [*Partington*, 2000]. Higher resolution optical and infra-red data became available through the DMSP Operational Linescan System (OLS), although this was limited by cloud cover. By 1994, some initial use was being made of the European Space Agency ERS-1 synthetic aperture radar observations of the ice edge. To supplement these data, the analysts have had opportunistic access to airborne and ship-borne reconnaissance data, as well as weather forecasts and their own ice charts from the previous week and ice charts and aerial reconnaissance maps provided by the ice services of other nations (e.g., Canada, Japan, Denmark, and Germany). The analysis procedure involves the use of high-resolution observations in preference to lower-resolution observations, so passive microwave sea ice concentrations were used in the analysis procedure only where all other forms of data were not available.

[7] For analysis of trends and modes of variability of the ice in the NIC ice chart record, it is important to emphasize that the quality and variety of the input data, and the general level of experience of the analysts in interpreting these data, changed over the period of the record, and it is very difficult if not impossible to establish a specific guideline on the quality of the data set, which will vary over time and according to location. Limitations of the data to be aware of are as follows.

[8] 1. Analysts have differing levels of experience, attention span, motivation, knowledge and skill and most were on a 3-year job rotation. The estimated precision in ice concentration estimation from this manual process is ±10%, and there remains the possibility of systematic biases in ice

concentrations from visual underestimation or overestimation by analysts.

[9] 2. Before 1976 and after 1986, pack ice was typically labeled as being 9 to 10 tenths ice concentration in the absence of detailed image data. Around 1976, the convention changed to labeling pack ice 10 tenths ice concentration. This does not significantly impact on the analysis presented in this study because it affects ice concentrations only in regions of very high ice concentration, which contribute insignificantly to the variance in the empirical orthogonal functions (EOFs) presented here. A change from concentrations being assigned in eighths to tenths also occurred.

[10] 3. The general level of expertise increased, which created its own possible biases. The quality of the NIC ice charts may be expected to have improved during the period, but at the same time systematic changes in the quality may be accompanied by biases in trends and patterns.

[11] 4. There are some potential errors in transferring information onto the original hardcopy ice charts and thence to the digital products used as the basis for the present study. This has been minimized and possibly rendered insignificant for large-scale analysis by several iterations of quality checking and correction of the data set, although any manual analysis procedure is bound to include some "typo" errors. No errors of this type were identified in the course of this work.

[12] 5. Changes have occurred in the quality of primary data sources used for the ice charts. Early on, during the 1970s in particular, there was a reliance on perceived climatology where appropriate data were unavailable. By the end of the period, the combination of improved weather forecasts, passive microwave ice concentrations, occasional SAR data, AVHRR and OLS data meant that the analysis procedure was much more robust and relied very little on climatology.

[13] Although it is difficult to validate these ice chart ice concentrations convincingly, given the fact that no other independent and better quality observations have been available with comparable coverage, the ice charts do represent a form of highly skilled manual "data assimilation." They are possibly the most informative and reliable record of sea ice conditions available across the Northern Hemisphere as a whole during the satellite era, almost certainly during summer when the passive microwave algorithms underestimate ice concentrations significantly.

2.3. Preparation of NIC Ice Chart Data

[14] The ice charts are available in Equal Area Scalable Earth (EASE) projection on CD-ROM from the National Snow and Ice Data Center (NSIDC) in Boulder, Colorado [*Armstrong and Brodzik*, 1995]. There are 1199 ice charts in the entire series covering 1972–1994, with each chart covering the area north of 45°N, consisting of 361 × 361 pixels. The pixel values are given in a sea ice code that expresses a range of ice concentrations, in tenths. The range relates to the uncertainty estimated by NIC for the ice concentrations and is in general between ±5% and ±10%.

[15] Mean values of these ranges were used for the analysis. Thus a value of "89" in an ice chart indicates 8 to 9 tenths ice concentration (uncertainty of ±5%), which is converted to 85% ice concentration for the purposes of this analysis. The change in convention of labeling pack ice concentrations (the second point above) is corrected in the data in a relatively crude fashion by replacing all ten tenths ice concentration pixels by 9–10 tenths (treated as 95% concentration in the analysis). Fast ice pixels (ice code "8") are treated as 100% concentration.

[16] Our analysis techniques allow gaps in the temporal sampling, but they must be at the same times for all pixels. It is therefore necessary to remove missing pixels ("no data" ice code) from the charts. Almost all the charts have a few missing pixels (mostly near land), and a few charts have many of them. We removed the fifty charts with the largest number of missing pixels from the data set, along with the pixels that have missing values in any of the remaining charts. This procedure removes only a small fraction of the data and creates only isolated gaps in spatial and temporal coverage. We therefore consider it preferable, in analysis of the full data set, to the interpolation that would otherwise be necessary. Pixel-wise linear interpolation over missing charts is used in preparing the 4-week and 52-week averaged data.

3. Modes of Hemispheric Sea-Ice Variability

[17] We now turn to the main purpose of this paper, which is to investigate modes of variability of the sea ice record and to relate these to particular Arctic climate processes that involve sea ice. For this, Empirical Orthogonal Function (EOF) analysis is used. In EOF analysis, a time-varying spatial signal is expressed as a sum of uncorrelated patterns using an orthogonal decomposition of the space-time data matrix. Each pattern is specified by a time series and a spatial pattern (EOF) that is multiplied by the time series. Under suitable conditions, the strongest EOFs correspond to independent, coherent modes of variability of the data over time. The analysis acts as a filter, separating the structured modes from noise and random variations.

[18] The technique is powerful as a tool for extracting modes of variability from the data, but it does have limitations that need to be recognized. EOF analysis assumes that the modes of variability are orthogonal to each other in time and space. Real climate modes of variability can be correlated, though distinct. Therefore it cannot be guaranteed that EOF modes represent the physical expression of independent processes. Lower-order modes are especially susceptible to contamination by high-order modes. This can create spatially remote correlations in the EOFs that do not necessarily correspond to real teleconnections. In short, EOF analysis can provide insight into modes of variability but must be used with care.

3.1. Empirical Orthogonal Function Analysis

[19] As our interest is in analyzing anomalies of ice concentration, the seasonal average is removed from the data prior to EOF analysis. This is done by computing the weekly mean concentration for each pixel, then subtracting the appropriate mean from each data sample, leaving a time series of anomalies for each pixel. The result of this preprocessing is a large space-time data matrix (26,165 pixels × 1149 charts). Its temporal covariance is the matrix of sums of pixel-wise cross-products for each pair of charts. The eigenvectors of this matrix are the EOF-related time

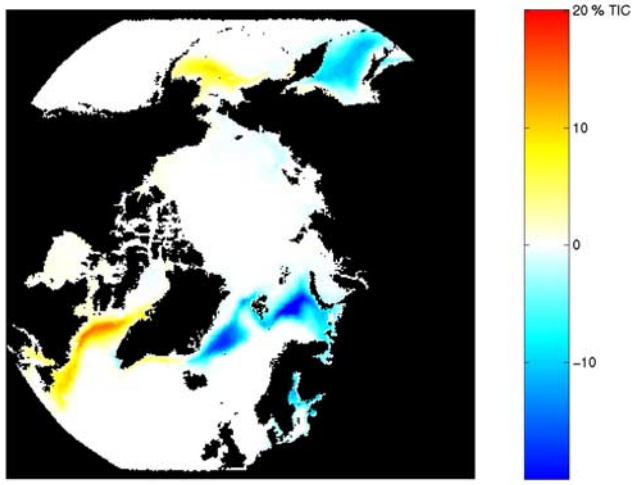

Figure 2. Empirical orthogonal function (EOF) 1, showing distribution of positive (red) and negative (blue) peaks corresponding to a positive phase of the pattern.

series. Each spatial EOF is computed by multiplication of the data matrix by the corresponding time series.

[20] The results of the EOF analysis are expressed in terms of the following:

[21] 1. Maps of the spatial EOFs, with blue (respectively red) indicating anomalous low (respectively high) ice concentrations when the time series is positive (Figures 2 and 3).

[22] 2. The standard deviation of the time series as a function of time of year. The season when the pattern is most active is indicated by high standard deviations (Figures 4 and 5).

[23] 3. The autocorrelation function of the time series, indicating its year-to-year variability and long term periodicity. Note that with a 23-year record, periods longer than about 10 years cannot be detected (Figures 6 and 7).

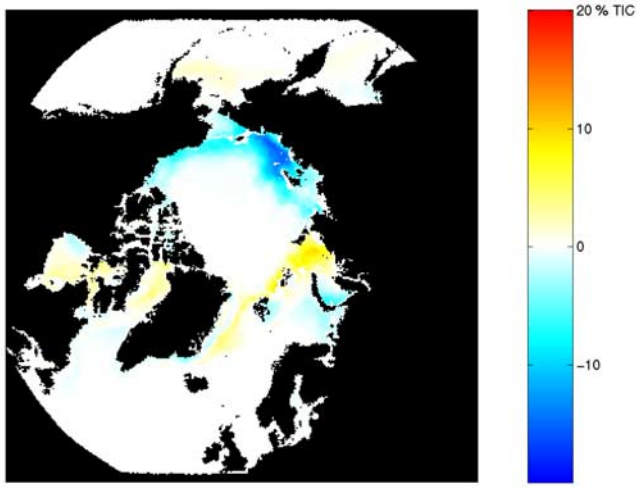

Figure 3. EOF 3, showing distribution of positive (red) and negative (blue) peaks corresponding to a positive phase of the pattern.

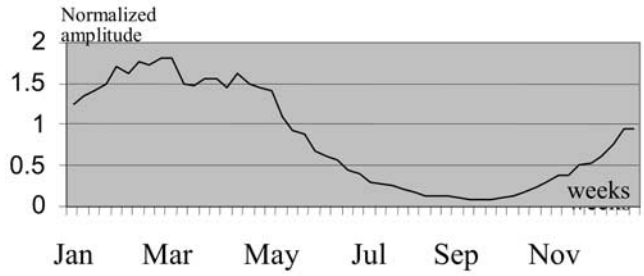

Figure 4. Seasonal standard deviation of EOF 1, showing the time of year when the pattern is most active.

[24] 4. The yearly extrema (samples with largest absolute value) of the time series, shown in relation to other parameters (Figures 8, 9, and 10).

3.2. General Results

[25] Table 1 shows the variance explained by the three main EOFs of the entire dataset, as a function of the degree of temporal averaging of the data. Each EOF as listed in the table shares common temporal and spatial characteristics at different degrees of averaging so these modes are relatively insensitive to the presence of high frequency week-to-week "noise" (43% of the variance is found at frequencies less than 4 weeks). The first two EOFs have large-scale hemispheric signatures with time series strongly concentrated in winter (Figure 4 for EOF 1). The spatial expression of EOF 1 is shown in Figure 2. EOF 2 is not presented here as it is artificially constrained by EOF 1 (both having variance concentrated in winter) and there is a strong possibility that it is an artifact of the technique for this reason. The third EOF, however, has a strong summer temporal signature (Figure 5). It is concentrated in the eastern (Eurasian) Arctic (Figure 3). EOF 3, being confined to the summer, is not constrained by EOFs 1 and 2 and hence is likely to provide useful insight into a key summer process. Lower-order EOFs explain progressively less variance, generally have less distinctive seasonal signatures and less hemispheric significance, and are increasingly artificially constrained by higher EOFs and so are not presented here. We therefore present EOFs 1 and 3 and discuss these in detail.

3.3. EOF 1: Winter Ice Anomalies Related to the North Atlantic Oscillation

[26] Figure 2 shows that EOF 1 has positive centers of activity in the Labrador Sea and Bering Sea and negative

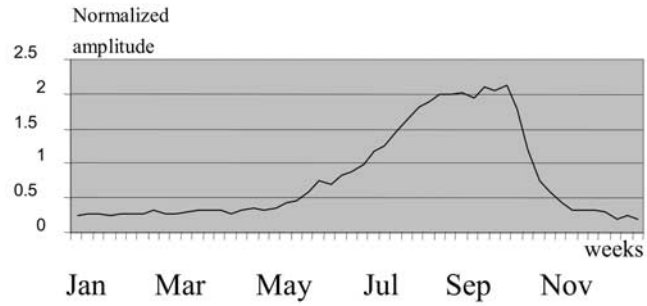

Figure 5. Seasonal standard deviation of EOF 3, showing the time of year when the pattern is most active.

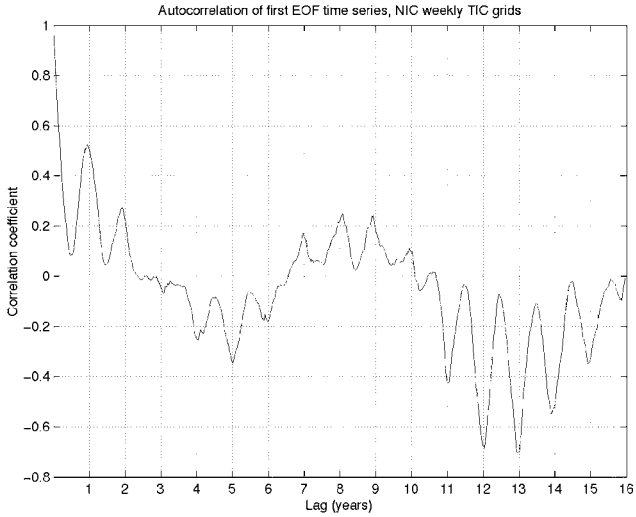

Figure 6. Autocorrelation function of EOF 1, showing year-to-year and multiyear correlation. Periods above about 10 years are not reliable due to the 23-year length of the record.

centers of activity across the North Atlantic (Greenland and Barents seas) and Sea of Okhotsk, and these centers of activity act in a dipole-like fashion. This is the North Atlantic Oscillation mode of variability found by *Cavalieri and Parkinson* [1987] among others. This mode of variability explains 9.7% of the total ice concentration variance of 4 week average anomalies and 24.3% of the annual average. Figure 4 shows that it is a winter phenomenon. There is a hint of a periodicity at about 8.5 years, but the length of the record does not provide much support for this. There is a moderately high winter-to-winter correlation of 0.5. The standard deviations of the ice concentration anomalies associated with this pattern are 21.6% at the negative peak (blue in Figure 2) and 15.5% at the positive

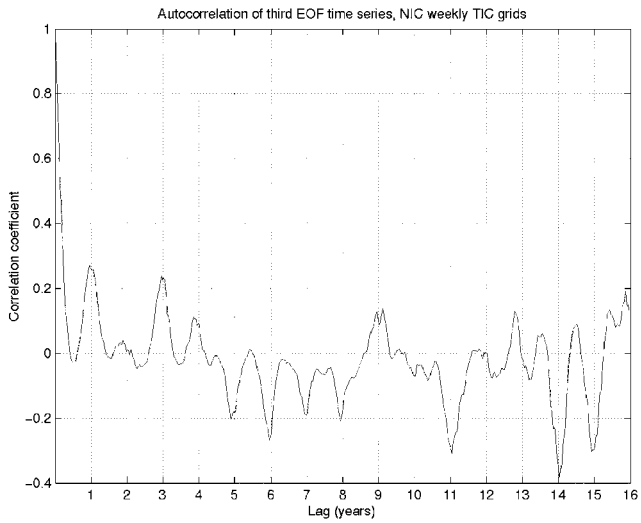

Figure 7. Autocorrelation function of EOF 3, showing year-to-year and multiyear correlation. Periods above about 11 years are not reliable due to the 23-year length of the record.

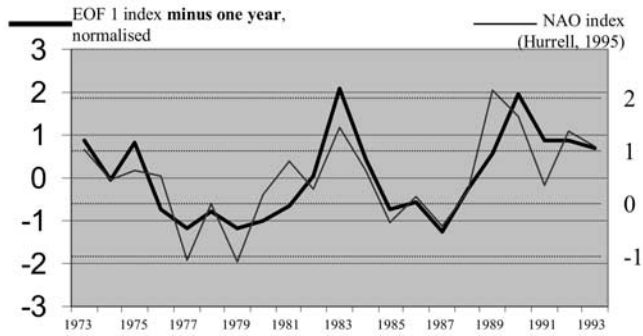

Figure 8. Time profile of the EOF 1 annual maximum amplitude to the 1-year delayed North Atlantic Oscillation index (NAO, after *Hurrell* [1995]).

peak (red). Recall that the polarities of these peaks change with the polarity of the time series (red is positive when the time series is positive) and are always opposite to each other.

[27] A comparison of the time series of this EOF to the North Atlantic Oscillation (NAO) from the previous year (Figure 8) provides a correlation coefficient of 0.80, which is significant at the 99% level. The NAO as published by James Hurrell [*Hurrell*, 1996] is an index of the normalized sea level pressure difference between Lisbon and Stykkisholmur, and is defined here as the maximum amplitude value of the winter (December to March) labeled as the year in which January falls. Furthermore, a regression of the January–March average total ice concentration fields onto the NAO of the previous year yields an even higher correlation of 0.90 with the spatial pattern of EOF 1. These correlations are therefore taken to indicate that the winter sub-polar seas respond clearly to the NAO after a lag of 1 year. The built-in delay in the system indicates that the NAO impacts on the distribution of perennial ice in the Arctic, which after a year impacts on marginal seas, particularly the Greenland Sea, via efflux through the Fram Strait. *Vinje* [2001] found that just such a 1-year lag was required to maximize the correlation of Fram Strait efflux with Arctic-wide perennial ice concentration estimates from *Johannessen et al.* [1999]. Thus, it is considered here that the ice coverage anomalies in the marginal polar seas detected in this most significant mode of ice concentration variability are the result of the impact of NAO-driven

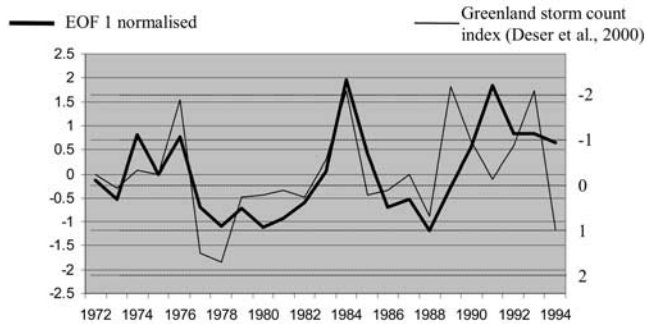

Figure 9. Time profile of EOF 1 annual maximum amplitude to Greenland Sea cyclone count from *Deser et al.* [2000].

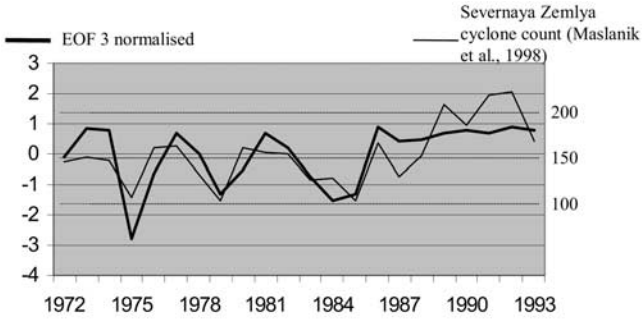

Figure 10. Time profile of the amplitude of EOF 3 shown plotted against number of cyclones recorded at Severnaya Zemlya (*Maslanik et al.* [1996], after *Serreze* [1994]).

atmospheric anomalies on the following year's ice cover (although the link of the NAO to Fram Strait ice flux has been demonstrated not to be robust on decadal timescales [*Jung and Hilmer*, 2001]). Interestingly, the Arctic Oscillation with a lag of 1 year generates a correlation of 0.39, which is significant at the 95% level, but much weaker than the correlation with the NAO, even though the Arctic Oscillation and EOF 1 are hemispheric in coverage and the NAO is regional. This reflects the fact that the bulk of the variability associated with EOF 1 lies in the North Atlantic region and the Pacific region dipole is weaker in amplitude. Thus, although EOF 1 is a hemispheric pattern, the main activity is in the Atlantic sector.

[28] There is evidence of feedback to heat flux into the atmosphere through a relationship of EOF 1 to cyclone count (Figure 9). The cyclone count in the Greenland Sea, as summarized by *Deser et al.* [2000, Figure 10] correlates significantly at the −0.57 level with the intensity of EOF 1. When there is a positive ice anomaly in the Greenland Sea, there is a reduced number of cyclones in the Greenland Sea. There is no lag with EOF 1, and we suggest that this is a response of the atmosphere to the ice coverage rather than the other way around, as the ice coverage is itself clearly a lagged response to the NAO.

3.4. EOF 3: Summer Sea-Ice Response to Preconditioning From the NAO in the Eastern Arctic

[29] EOF 3 is a predominantly eastern Arctic expression (Figure 3) and is a summer phenomenon (Figure 5). It is expressed as a negative sea ice anomaly in the Beaufort, East Siberian, and Laptev Seas, and a positive anomaly in northern Kara Sea. The standard deviations of ice concentration anomaly associated with this pattern are 15.9% at the negative peak (blue in Figure 3) and 10.3% at the positive peak (red). Temporal behavior is illustrated in Figures 7 and 10.

Table 1. Variance of Three Principal EOFs Versus Amount of Averaging, From None (Weekly Ice Charts) Through 4 Weeks to 52 Weeks[a]

	Weekly	Four-Week Average	Annual Average
EOF 1% variance	6.8	9.6	24.3
EOF 2% variance	3.1	4.2	10.6
EOF 3% variance	2.8	4.5	9.3
Total	12.7	18.3	44.2

[a]EOF 2 is not discussed in this paper.

[30] This pattern is closely connected to the reduction in summer ice coverage in the East Siberian Sea that has been well publicized in the literature [e.g., *Maslanik et al.*, 1996]. It appears from our results that there may be conditioning from the previous winter as there is a correlation, significant at the 90% level, with ice drift anomalies from 6 months earlier (Figure 11). Ice drift anomalies are computed from the ice drift data set generated by W. Emery and colleagues at the University of Colorado, to be available in the near future through NSIDC. There is also a correlation of 0.32 with the NAO from the previous winter, which is significant at the 90% level. This therefore confirms the results of *Rigor et al.* [2001], who found similar results from an analysis of buoy data. Similarly, associated with spring sea level pressures, *Deser et al.* [2000] find an anomalous northerly wind over the Kara Sea associated with positive summer ice anomalies and anomalous southerly spring winds over the Laptev and East Siberian Seas associated with negative summer ice anomalies. It is suggested that sea level pressure anomalies from winter and spring cause an export of ice from the East Siberian and Laptev Seas during the positive phase of the NAO and at the same time an import in the northern Kara Sea, where Severnaya Zemlya acts to block the dispersion of the ice causing a build-up (the south Kara Sea is an exporter of ice). These ice anomalies provide preconditioning for summer ice anomalies.

[31] As for EOF 1, we are also seeing in this EOF direct links between summer ice conditions and summer cyclone counts (Figure 10). Not only is there a generally very good correlation between the intensity of this pattern and the total number of cyclone counts, at least up to about 1989, but the spatial distribution is consistent, too. EOF 3 is correlated with the cyclone count at 75°N–90°N, 60°E–160°E during April–September, 1972–1993, to a level of 0.7 (cyclone counts from *Maslanik et al.* [1996], based on work by *Serreze* [1994]). *Maslanik et al.* [1996] contrast the periods 1982–1987 with 1988–1993 to investigate the spatial distribution of changes in cyclone counts in summer. The

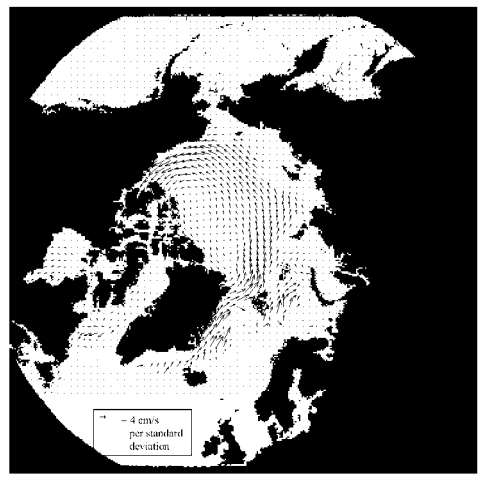

Figure 11. Ice drift anomalies associated with EOF 3 summer ice concentration variability, from the previous winter. The units are cm/s of drift velocity per standard deviation of the EOF time series.

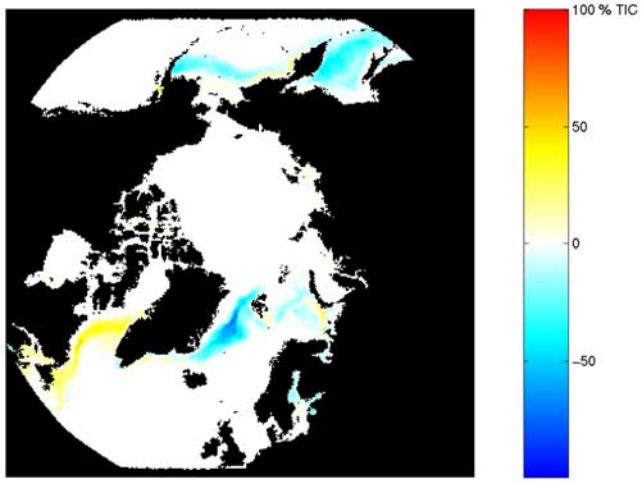

Figure 12. Linear reduction in ice concentrations in the Northern Hemisphere, 1972–1994, in winter.

period 1982–1988 was generally a period of negative phase for this pattern, while 1988–1993 was a period of high positive phase (Figure 10). While there is a general increase in the cyclone activity in the East Siberian and Laptev Seas from 1982–1987 to 1988–1993 as the negative sea ice anomaly grew, there is a reduction in the cyclone activity over the same period in the Kara Sea where the positive anomaly developed (Figure 11 here, and Figure 5 of *Maslanik et al.* [1996]). The strong possibility here is that the conditioning from the previous winter ice advection causes enhanced heat flux from the ocean which itself results in an enhanced frequency of cyclones passing into the Arctic from the south, as well as reduced summer ice coverage. As *Deser et al.* [2000] point out, ice cover changes can result in heat flux anomalies of the order of 200 to 250 W m^{-2} which are an order of magnitude larger than the effects of a 0.5°C sea surface temperature anomaly in midlatitudes. They hypothesize that a similar ice coverage led process of storm track influence is at play in east Greenland. According to *Rigor et al.* [2001], the increased latent heat resulting from this decrease in ice coverage is at least in part responsible for the increased winter temperatures in this region.

3.5. Discussion

[32] This analysis has demonstrated how the NAO has a lagged and broad influence on sea ice coverage in the Northern Hemisphere. The major modes of ice variability in both summer and winter are influenced by the NAO, the winter mode overwhelmingly and the summer mode less strongly. The NAO can, to large extent in winter, be used to forecast general sea ice conditions, while this may also be the case in summer, with much less reliability. Results are also presented which suggest how the sea ice feeds back to the atmosphere, through an influence on cyclone frequencies both in summer in the Siberian shelf region, and in winter in the Greenland Sea. In the case of the winter mode of sea ice variability, this is probably a feedback from the sea ice as the sea ice coverage is determined by the NAO from the previous year. In the case of the Siberian shelf region, the evidence is less strong as a result of the weaker (though still significant) influence of the NAO from the previous winter.

[33] Figures 12 and 13 show the linear trend in ice concentrations from 1972–94. The pattern of winter reduction in ice coverage matches well with a strengthening of EOF 1, the NAO sea ice signature. The exception to this is the Bering Sea where ice cover has decreased despite a strengthening of EOF 1 which, on its own, suggests an increase in Bering Sea ice coverage. This could indicate that the apparent connectivity between the Pacific and Atlantic sectors in the EOF analysis is less strong than is indicated, with the Atlantic sector being dominated in winter by the NAO and the Pacific sector, particularly the Bering Sea, being dominated by other processes (compare Figure 12 with Figure 2). However, it is important to note that the NAO will not necessarily remain robust as a forecaster of ice conditions.

[34] The linear trend in summer ice coverage shows a strong reduction in the East Siberian Sea region, which reflects EOF 3 and its strengthening, although the corresponding increase in ice coverage in the Kara Sea in EOF 3 is not reflected in the linear trend. Interestingly, the linear trend in summer is very highly dominated by conditions in the East Siberian Sea. Elsewhere, the pattern of change is fairly neutral on balance.

[35] There is a hint that the relationship between cyclone frequencies and the NAO-related EOF amplitudes, i.e., an element of ice-related atmospheric feedback, may have broken down from 1989 (Figures 9 and 10). Given the length of this record, which ends in 1994, there is insufficient data to determine whether this is real or not. Suffice it to say that there were a large number of well documented changes in the Arctic around 1989, including a move to a notably cyclonic mode of ice drift with a lower central Arctic sea level pressure and sea level [*Johnson et al.*, 1999]. A proper assessment of this will require data from after 1994.

4. General Conclusions

[36] National Ice Center ice charts provide a valuable record of ice conditions for those interested in high latitude

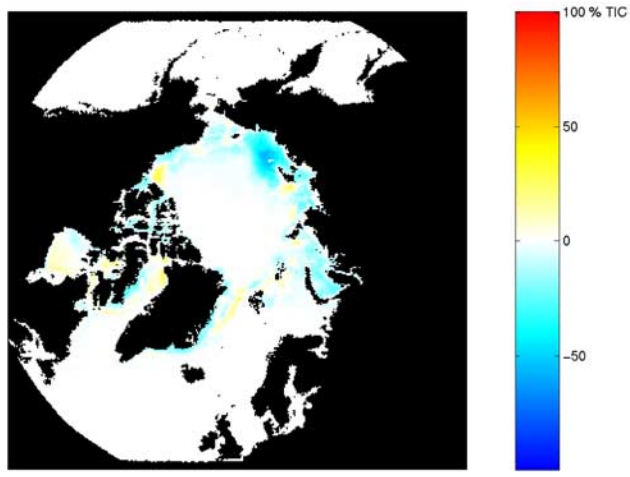

Figure 13. Linear reduction in ice concentrations in the Northern Hemisphere, 1972–1994, in summer.

climate. EOF analysis reveals modes of variability that have important implications for the nature of inter-annual climate variability in the Arctic. This analysis also goes some way to identifying key modes of variability that contributed to the significant reduction in sea ice the Arctic during the last quarter of the twentieth century.

[37] The key results of this study are as follows.

[38] 1. Two principal modes of variability in ice concentration in the peripheral Arctic seas are related to (1) lagged effect on winter ice concentrations of large-scale pressure anomalies associated with the NAO (EOF 1) and (2) NAO-related preconditioning of summer ice conditions in the eastern Arctic (EOF 3).

[39] 2. Evidence is presented that these ice concentration anomalies appear, in turn, to determine heat flux and cyclone distributions and intensities, both in the Greenland Sea in winter and the Siberian Shelf region in summer, although there is also evidence that this breaks down during the strong cyclonic phase of Arctic circulation [*Johnson et al.*, 1999].

[40] 3. The NAO has potential to assist in seasonal forecasting of winter and, to lesser extent, summer ice conditions. It must be taken into account, however, that the variance not explained by the two key EOFs is significant both in winter and in summer and so will add significant interannual ''noise'' to any seasonal prediction.

[41] The impact of the NAO on both winter and summer modes of sea ice variability in the Northern Hemisphere is not necessarily robust on interdecadal timescales. The discontinuous Fram Strait ice flux relationship to the NAO provides a cautionary tale in this regard [*Kwok and Rothrock*, 1999; *Hilmer et al.*, 1998]. It is therefore important to continue to monitor the relationship between the NAO and ice concentration to establish whether the relationship is maintained. If it is not maintained, then this may indicate a major ''flip'' in the dynamics of the Arctic climate system.

Appendix A: Notes on Differences of NIC Ice Charts to Passive Microwave (NASA Team) Sea Ice Record

[42] This analysis has been based on ice chart data rather than the more commonly analyzed passive microwave derived ice concentrations. Differences between the NIC ice chart sea ice record and the passive microwave sea ice record are highly significant despite the fact that the NIC charts are semi-dependent on the passive microwave data, and it is worth noting these differences. We compare the ice chart data to ice concentrations from the NASA Team algorithm which, along with the Bootstrap algorithm [*Comiso*, 1995], has proved to be perhaps the most popular used for generating ice concentrations [*Cavalieri et al.*, 1997]. We find a baseline difference in integrated ice concentration coverage north of 45°N of 3.85% ± 0.73% during November to May (ice chart concentrations are larger). In summer, the difference between the two sources of data rises to a maximum of 23% peaking in early August, equivalent to ice coverage the size of Greenland.

[43] The differences in trends between the two data sets have also been investigated, as this has implications for climate studies. The trends are calculated by applying a linear fit to integrated ice concentration across the Northern Hemisphere (with the passive microwave ''pole hole'' filled with 100% ice cover). The period is 1979–1994, which is the period of overlap of the two sensors. Table A1 shows that there is a very modest (statistically insignificant) difference in integrated sea ice concentration trend in winter between 1979 and 1994. However, in summer (weeks 24 to 36), there is a statistically significant difference, with the gradient being −4.88% per decade for the NIC data and −6.98% per decade for the NASA Team data.

Table A1. Linear Trends in Integrated Ice Coverage From the NASA Team Algorithm and the NIC Ice Chart Data for the Overlap Period, 1979–1994, for Summer, Winter, and the Whole Year[a]

1979–1994 Linear Trends	Winter, Weeks 1–23; 37–52	Summer, Weeks 24–36	Annual, All Weeks
NIC	−1.58	−4.88	−2.27
NASA Team	−1.37	−6.98	−2.90

[a]Figures are percentage change per decade.

[44] **Acknowledgments.** This study was sponsored by Naval Research Laboratories contract N00173-01-P-6204 and NASA grant NAG5-11367 from the Cryospheric Program. The important role of the analysts at the National Ice Center and Veridian-ERIM International is acknowledged in quality assessing and correcting this data set over many iterations.

References

Armstrong, R. L., and M. J. Brodzik, An Earth-gridded SSM/I data set for cryospheric studies and global change monitoring, *Adv. Space Res.*, *10*, 155–163, 1995.

Benner, D., and C. Bertoia, Operational satellite sea ice analysis at the Navy/NOAA Joint Ice Center, paper presented at 6th Conference on Satellite Meteorological and Oceanography, Am. Meteorol. Soc., Atlanta, Georgia, Jan. 5–10, 1992.

Benner, D., and R. Ramsay, Ice hazard team report, report, CEOS/IGOS Disaster Manage. Support Project, Washington, D. C., 2000.

Cavalieri, D. J., and C. L. Parkinson, On the relationship between atmospheric circulation and the fluctuations in the sea ice extents on the Bering and Okhotsk seas, *J. Geophys. Res.*, *92*(C7), 7141–7162, 1987.

Cavalieri, D. J., P. Gloersen, C. L. Parkinson, J. C. Comiso, and H. J. Zwally, Observed asymmetry in global sea ice changes, *Science*, *278*, 1104–1106, 1997.

Comiso, J. C., SSM/I concentrations using the Bootstrap algorithm, *NASA RP 1380*, 40 pp., NASA Goddard Space Flight Cent., Greenbelt, Md., 1995.

Dedrick, K., K. Partington, M. Van Woert, C. Bertoia, and D. Benner, U. S. National/Naval Ice Center digital sea ice data and climatology, *Can. J. Remote Sens.*, *27*(5), 457–475, 2001.

Deser, C., J. E. Walsh, and M. S. Timlin, Arctic sea ice variability in the context of recent atmospheric circulation trends, *J. Clim.*, *13*, 617–633, 2000.

Hilmer, M., M. Harder, and P. Lemke, Sea ice transport: A highly variable link between Arctic and North Atlantic, *Geophys. Res. Lett.*, *25*(17), 3359–3362, 1998.

Hollinger, J. R., R. Lo, G. Poe, R. Savage, and J. Pierce, Special sensor microwave/imager calibration/validation, final report, pp. 10.1–10.20, Nav. Res. Lab., Washington, D. C., 1991.

Hurrell, J., Decadal trends in the North Atlantic Oscillation: Regional temperatures and precipitation, *Science*, *269*, 676–679, 1995.

Hurrell, J., Influence of variations in extratropical wintertime teleconnections on Northern Hemisphere temperature, *Geophys. Res. Lett.*, *23*, 665–668, 1996.

Johannessen, O., M. Miles, and E. Bjorgo, The Arctic's shrinking sea ice, *Nature*, *376*, 126–127, 1995.

Johannessen, O., E. V. Shalina, and M. Miles, Satellite evidence for an Arctic sea ice cover in transformation, *Science*, *286*, 1937–1939, 1999.

Johnson, M. A., A. Y. Proshutinsky, and I. V. Polyakov, Atmospheric patterns forcing two regimes of Arctic ice-ocean circulation: A return to anticyclonic conditions?, *Geophys. Res. Lett.*, *26*(11), 1621–1624, 1999.

Jung, T., and M. Hilmer, The link between the North Atlantic Oscillation and arctic sea ice export through Fram Strait, *J. Clim.*, *14*, 3932–3943, 2001.

Kwok, R., and D. A. Rothrock, Variability of Fram Strait ice flux and North Atlantic Oscillation, *J. Geophys. Res.*, *104*(C3), 5177–5189, March 15, 1999.

Maslanik, J. A., M. C. Serreze, and R. G. Barry, Recent decreases in Arctic summer ice cover and linkages to atmospheric circulation anomalies, *Geophys. Res. Lett.*, *23*(13), 1677–1680, 1996.

Partington, K. C., A data fusion algorithm for mapping sea ice concentrations from SSM/I data, *IEEE Trans. Geosci. Remote Sens.*, *38*(4), 1947–1958, July 2000.

Rigor, I. G., J. M. Wallace, and R. Colony, On the response of sea ice to the Arctic Oscillation, *J. Clim.*, *15*, 2648–2668, 2001.

Rothrock, D. A., Y. Yu, and G. A. Maykut, Thinning of the Arctic sea-ice cover, *Geophys. Res. Lett.*, *26*(23), 3469–3472, 1999.

Serreze, M., Climatological aspects of cyclone development and decay in the Arctic, *Atmos. Ocean.*, *33*, 1–23, 1994.

Vinje, T., Fram Strait ice fluxes and atmospheric circulation, *J. Clim.*, *14*, 3508–3517, 2001.

C. Bertoia, Cospas-Sarsat Secretariat, 99 City Road, London EC1Y 1AX, UK. (cheryl_bertoia@imso.org)

K. Dedrick and D. Lamb, National/Naval Ice Center, 4251 Suitland Road, Washington, DC 20395, USA. (lambd@natice.noaa.gov)

T. Flynn, Vexcel Corporation, 4909 Nautilus Court, Boulder, CO 80301, USA. (tom.flynn@vexcel.com)

K. Partington, Vexcel UK, Arrowfield House, 6 Pound St., Newbury, Berkshire RG14 6AA, UK. (kim.partington@vexcel.co.uk)